Oxygen Sensors Based on Mesoporous Silica Particles on Layer-by-Layer Self-assembled Films

Bao-Hang Han, Ian Manners, and Mitchell A. Winnik*

Department of Chemistry, University of Toronto, 80 St. George Street, Toronto, Ontario M5S 3H6, Canada

Received December 20, 2004. Revised Manuscript Received March 7, 2005

We describe photoluminescent (PL) oxygen sensors based upon phosphorescent dyes adsorbed into the pores of mesoporous silica particles at submonolayer coverage on a layer-by-layer self-assembled film. Eight transition metal dyes (four Pt and Pd porphyrin complexes and four ruthenium complexes) were investigated through monitoring the changes in PL intensity and lifetime upon varying oxygen pressure. The intensity Stern−Volmer (SV) plots were curved. In most systems, the intensity SV plots match the lifetime SV plots, with deviations seen only at high oxygen pressures where static quenching may play a role. The curved intensity Stern−Volmer plots could be fitted with two phenomenological models, a two-site model, and a model based on a Freundlich binding isotherm for oxygen. The Gaussian distribution model was less successful in fitting the data. The most important result to emerge from these data is that the unquenched lifetime of the dye itself is not a sufficient scaling parameter to reduce all of the SV plots to a common line. A second scaling parameter was necessary. This parameter, which measures the capture radius for quenching (R_{eff}), times the efficiency of quenching per encounter α ranged from 0.38 nm for PdOEP and 0.42 for PtTPP to 1.12 for $Ru(bpy)_3]Cl_2$ and 1.25 for $Ru(phen)_3]Cl_2$ relative to an assumed value of $\alpha R_{eff} = 1.0$ nm for PtOEP.

Introduction

Over the past 20 years, scientists have been interested in developing oxygen sensors based upon the principle that oxygen is a powerful quencher of the electronically excited state of dyes. The dyes are normally incorporated into polymer films, often as a true solution, but sometimes adsorbed onto colloidal silica particles dispersed in the film. These dye-containing films act as sensors because oxygen diffuses from the surrounding medium into the film. Most of the dyes that have been successfully employed as oxygen sensors exhibit phosphorescence at ambient temperature.[1] The most commonly used dyes for these applications have been transition metal porphyrin derivatives such as platinum and palladium porphines,[2−9] and ruthenium polypyridyl or phenanthroline complexes.[10−17] The most common polymer matrixes have been silicone polymers,[6,10−12,17] chosen for their high oxygen permeability. Our research group has examined the properties of poly(aminothionylphosphazene)s (PATP)[18−25] as useful matrixes for dye-based oxygen sensor applications. Other polymers that have been examined include polystyrene (PS),[2,7−9,11,12] poly(vinyl chloride) (PVC),[5,11] cellulose deriva-

* To whom correspondence should be addressed. E-mail: mwinnik@chem.utoronto.ca.

(1) (a) Amao, Y. *Microchim. Acta* **2003**, *143* (1), 1−12. (b) Bell, J. H.; Schairer, E. T.; Hand, L. A.; Mehta, R. D. *Annu. Rev. Fluid Mech.* **2001**, *33*, 155−206. (c) Lu, X.; Manners, I.; Winnik, M. A. In *New Trends in Fluorescence Spectroscopy*; Valeur, B., Brochon, J.-C., Eds.; Springer-Verlag: Berlin, 2001; pp 229−255. (d) Lu, X.; Winnik, M. A. In *Organic, Physical, and Materials Photochemistry*; Ramamurthy, V., Schanze, K. S., Eds.; Marcel Dekker Inc.: New York, 2000; pp 311−352. (e) Lu, X.; Winnik, M. A. *Chem. Mater.* **2001**, *13* (10), 3449−3463. (f) Demas, J. N.; DeGraff, B. A. *J. Chem. Ed.* **1997**, *74* (6), 690−695. (g) Gouterman, M. *J. Chem. Ed.* **1997**, *74* (6), 697−702. (h) Guillet, J. E.; Andrews, M. *Macromolecules* **1992**, *25* (10), 2752−2756.
(2) Papkovsky, D. B. *Sens. Actuators B* **1995**, *29*, 213−218.
(3) Mills, A.; Lepre, A. *Anal. Chem.* **1997**, *69* (22), 4653−4659.
(4) Amao, Y.; Asai, K.; Okura, I.; Shinohara, H.; Nishide, H. *Analyst* **2000**, *125*, 1911−1914.
(5) Douglas, P.; Eaton, K. *Sens. Actuators B* **2002**, *82*, 200−208.
(6) Lee, S.-K.; Okura, I. *Spectrochim. Acta A* **1998**, *54* (1), 91−100.
(7) Papkovsky, D. B.; Ponomarev, G. V.; Trettnak, W.; O'Leary, P. *Anal. Chem.* **1995**, *67* (22), 4112−4117.
(8) Hartman, P.; Trettnak, W. *Anal. Chem.* **1996**, *68* (15), 2615−2620.
(9) Papkovsky, D. B.; Ovchinnikov, A. N.; Ogurtsov, V. I.; Ponomarev, G. V.; Korpela, T. *Sens. Actuators B* **1998**, *51*, 137−145.
(10) Kilmant, I.; Wolfbeis, O. S. *Anal. Chem.* **1995**, *67* (18), 3160−3166.
(11) Mills, A. *Sens. Actuators B* **1998**, *51*, 60−68.
(12) Mills, A. *Sens. Actuators B* **1998**, *51*, 69−76.
(13) Matsui, K.; Sasaki, K.; Takahashi, N. *Langmuir* **1991**, *7* (11), 2866−2868.
(14) Castellano, F. N.; Heimer, T. A.; Tandhasetti, M. T.; Meyer, G. J. *Chem. Mater.* **1994**, *6* (7), 1041−1048.
(15) DellaGuardla, R. A.; Thomas, J. K. *J. Phys. Chem.* **1983**, *87* (6), 990−998.
(16) Wolfgang, S.; Gafney, H. D. *J. Phys. Chem.* **1983**, *87* (26), 5395−5401.
(17) Xu, W.; McDonough, R. C. III; Langsdorf, B.; Demas, J. N.; DeGraff, B. A. *Anal. Chem.* **1994**, *66* (23), 4133−4141.
(18) Yekta, A.; Masoumi, Z.; Winnik, M. A. *Can. J. Chem.* **1995**, *73* (11), 2021−2029.
(19) Pang, Z.; Gu, X.; Yekta, A.; Masoumi, Z.; Coll, J. B.; Winnik, M. A.; Manners, I. *Adv. Mater.* **1996**, *8* (9), 768−771.
(20) Masoumi, Z.; Stoeva, V.; Yekta, A.; Pang, Z.; Manners, I.; Winnik, M. A. *Chem. Phys. Lett.* **1996**, *261*, 551−557.
(21) Masoumi, Z.; Stoeva, V.; Yekta, A.; Winnik, M. A.; Manners, I. in *Polymers and Organic Solids*; Eds. Shi, L.; Zhu, D.; Science Press: Beijing, China, **1997**, pp157−168.
(22) Jayarajah, C. N.; Yekta, A.; Manners, I.; Winnik, M. A. *Macromolecules* **2000**, *33* (15), 5693−5701.
(23) Lu, X.; Manners, I.; Winnik, M. A. *Macromolecules* **2001**, *34* (6), 1917−1927.
(24) Wang, Z.; McWilliams, A. R.; Evans, C. E. B.; Lu, X.; Chung, S.; Winnik, M. A.; Manners, I. *Adv. Funct. Mater.* **2002**, *12* (6−7), 415−419.
(25) Lu, X.; Han, B.-H.; Winnik, M. A. *J. Phys. Chem. B* **2003**, *107* (48), 13349−13356.

10.1021/cm047770k CCC: $30.25
Published on Web 05/13/2005

tives (ethylcellulose (EC),[5] cellulose acetate butyrate (CAB)[3,5,11]), and poly(methyl methacrylate) (PMMA).[3,5] In addition, a number of inorganic substrates have been used.[13−16]

For dyes dissolved in simple fluid solvents or dissolved in polymer films at temperatures above the glass transition temperature of the polymer, we have a good understanding of the factors that affect the quenching kinetics. The key factors that play a role include the solubility of oxygen and the diffusion coefficient of oxygen in the host medium, and the excited state lifetime of the dye. For dyes that are adsorbed on solid substrates, we have a much poorer understanding of the factors that affect the quenching process. There have been relatively few studies. Researchers who have examined oxygen quenching for dyes adsorbed to solid substrates such as silica have found that the photoluminescence (PL) decay profile of the dyes, even in the absence of oxygen, are nonexponential. This result suggests that the dyes occupy a distribution of different sites on the surface, and that excited dyes at each type of site have their own characteristic decay rate.

In addition, one can imagine two distinct mechanisms for oxygen molecules in the gas phase to quench the excited states of dyes adsorbed to a surface. In the Langmuir-Rideal mechanism, collisions between O_2 molecules in the gas phase with excited dyes on the surface lead to quenching. One can think of this process as a kind of ballistic quenching process because it involves a direct encounter between a molecule of O_2 in the gas phase undergoing a mean-free-path excursion with a dye that is stationary on the substrate on the time scale of the collision. In the Langmuir−Hinshelwood mechanism, oxygen molecules adsorb to the surface of the substrate and undergo random diffusion on the surface prior to encountering the excited dye molecule. Here, among the important factors that affect the quenching kinetics are the binding isotherm of the O_2 molecules, the rate of surface diffusion, and the residence time of the O_2 molecules on the surface. The most detailed experiments to sort out these two quenching mechanisms have been those from the group of J. K. Thomas[26] at Notre Dame, who examined the quenching of the fluorescence by oxygen of two dyes, pyrene and 9,10-diphenylanthracene, with very different singlet excited-state lifetimes, adsorbed to the surface of a commercial nonporous silica. Their experiments provided strong support for the idea of preadsorption of O_2 molecules onto the silica surface as a key step in the quenching process. They also pointed out that the adsorption of other molecules onto the silica surface such as water or alcohols created obstacles for the surface diffusion of oxygen, leading to a decrease in the quenching rate.

In recent years, a need has been identified for optical oxygen sensors with very fast response times. These sensors, for example, would be able to monitor the propagation of shock waves across the body of an airplane breaking the sound barrier or due to an explosion. One might be interested in the propagation velocity of the initial shock wave or the consequences of the reflection of the shock wave off a variety of surfaces. For PL sensors based on dyes dissolved in liquid films, the response time is limited by the rather slow rate of diffusion of O_2 molecules in the film. Shock tube (pressure jump) experiments by the Sullivan group[27] at Purdue and the Amao group[28] in Japan have shown that solid substrates such as the alumina surface of anodized aluminum and the silica surface of commercial thin-layer chromatography plates provide more rapid response to sudden changes in oxygen partial pressure. These experiments emphasize the need for a better understanding of the factors that affect PL quenching by oxygen for dyes adsorbed to these surfaces.

Here we report our experiments in which we examine the quenching of phosphorescence of a series of different dyes adsorbed to a thin-film system which we hope will exhibit a rapid response to changes in oxygen pressure. The system consists of micrometer-size particles of nanoporous silica, attached at a submonolayer coverage to a thin polymer film prepared by layer-by-layer self-assembly.

Mesoporous silica materials have been known since 1992.[29] These materials are characterized by a huge surface area, a relatively large pore size, and a large pore volume. We have chosen SBA-15 mesoporous silica[30] as a promising candidate substrate in which dyes could be bound to the surface of the mesopores (around 8 nm in diameter). Because of the high surface-to-volume ratio, we imagined that a monolayer of micrometer-sized mesoporous silica particles could adsorb sufficient dye to produce a strong PL signal, and at the same time provide rapid access to oxygen molecules from the external atmosphere. To produce the thin film structure we desired, we took advantage of the anionic surface charge of the silica particles in combination with the properties of thin films produced by the layer-by-layer self-assembled film (LbLSAF) technique.[31] Using LbL assembly, we produced a thin hard polymer film with a net cationic charge. Exposure of this film to a suspension of the mesoporous particles led to single-layer adsorption at submonolayer coverage. As we describe below, dyes bound to these films have a sufficient PL intensity to allow them to be studied in much the same way as more macroscopic silica assemblies.

(26) Krasnansky, R.; Koike, K.; Thomas, J. K. *J. Phys. Chem.* **1990**, *94* (11), 4521−4528.
(27) (a) Sakaue, H.; Sullivan, J. P. *AIAA J.* **2001**, *39* (*10*), 1944−1949. (b) Sakaue, H.; Gregory, J. W.; Sullivan, J. P. *AIAA J.* **2002**, *40* (*6*), 1094−1098.
(28) Kameda, M.; Tezuka, N.; Hangai, T.; Asai, K.; Nakakita, K.; Amao, Y. *Meas. Sci. Technol.* **2004**, *15*, 489−500.
(29) (a) Beck, J. S.; Vartuli, J. C. *Curr. Opin. Solid State. Mater. Sci.* **1996**, *1*, 76−87. (b) Kresge, C. T.; Leonowicz, M. E.; Roth, W. J.; Vartuli, J. C.; Beck, J. S. *Nature* **1992**, *359*, 710−712. (c) Beck, J. S.; Vartuli, J. C.; Roth, W. J.; Leonowicz, M. E.; Kresge, C. T.; Schmitt, K. D.; Chu, C. T.-W.; Olson, D. H.; Sheppard, E. W.; McCullen, S. B.; Higgins, J. B.; Schlenker, J. L. *J. Am. Chem. Soc.* **1992**, *114* (27), 10834−10843. (d) Beck, J. S.; Vartuli, J. C.; Kennedy, G. J.; Kresge, C. T.; Roth, W. J.; Schramm, S. E. *Chem. Mater.* **1994**, *6* (10), 1816−1821. (e) Vartuli, J. C.; Schmitt, K. D.; Kresge, C. T.; Roth, W. J.; Leonowicz, M. E.; McCullen, S. B.; Hellring, S. D.; Beck, J. S.; Schlenker, J. L.; Olson, D. H.; Sheppard, E. W. *Chem. Mater.* **1994**, *6* (12), 2317−2326.
(30) (a) Zhao, D.; Feng, J.; Huo, Q.; Melosh, N.; Fredrickson, G. H.; Chmelka, B. F.; Stucky, G. D. *Science* **1998**, *279*, 548−552. (b) Zhao, D.; Huo, Q.; Feng, J.; Chmelka, B. F.; Stucky, G. D. *J. Am. Chem. Soc.* **1998**, *120* (24), 6024−6036. (c) Zhao, D.; Yang, P.; Huo, Q.; Chmelka, B. F.; Stucky, G. D. *Curr. Opin. Solid State Mater. Sci.* **1998**, *3*, 111−121.
(31) (a) Decher, G. *Science* **1997**, *277*, 1232−1237. (b) Groth, T.; Lendlein, A. *Angew. Chem., Ind. Ed.* **2004**, *43* (8), 926−928; *Angew. Chem.* **2004**, *116* (8), 944−946.

We report steady-state luminescence experiments and pulsed laser experiments to compare the susceptibility to quenching of a series of phosphorescent dyes on this substrate. Our approach to data analysis resembles that described by Carraway et al.[32] more than a decade ago, who studied oxygen quenching of several ruthenium dyes adsorbed into transparent porous silica disks prepared by compaction of porous commercial fumed silicas. Other publications that examine PL quenching experiments for dyes adsorbed to silica may be found in refs 13−16 and 33−35. Our experiments involve a different silica substrate and a larger selection of dyes, with a broad range of different lifetimes.

We also note that, at a recent conference in China, a poster was presented describing oxygen PL quenching experiments for ruthenium dyes adsorbed into MCM-41, a similar mesoporous silica, but with smaller pores.[36]

Experimental Section

Instrumentation. Samples prepared by spin coating employed a Headway Research, Inc., Model PWM32 spin coater. Nitrogen sorption (T = 77 K) isotherms were obtained with an AUTOSORB-1 automated gas adsorption analyzer (Quantachrome Instruments). The samples were degassed overnight at 200 °C. Isotherms were evaluated with the Barrett−Joyner−Halenda (BJH) theory[37] to give the porosities, including the Brunauer−Emmett−Teller (BET) surface area,[38] pore volume, pore size, and its distribution.[39] Scanning electron microscopy (SEM) images were acquired on an Hitachi S-5200 scanning electron microscope at an acceleration voltage of 10 kV. Mesoporous silica samples were suspended in deionized water, with ultrasonication. One drop of the suspension was applied to a 400 mesh carbon-coated copper grid and left to dry in the air. For the mesoporous silica particles on the LbLSAF sample, a piece of the slide (ca. 6 mm × 8 mm) was cut and attached to the SEM sample holder.

Luminescence spectra and intensities were obtained with a SPEX Industries Inc. Fluorolog II Model SPEX1680 spectrometer. Luminescence decay profiles were obtained with a home-built device using the third harmonic (355 nm) of a pulsed Nd:YAG laser (Spectra-Physics GCR-170) as the excitation source. The laser beam intensity was severely attenuated through a High-Energy Variable Attenuator (Newport, Model 935-10) to prevent sample damage and/or dye photobleaching. A filter BP300-400 was placed in the excitation beam path before the film sample, and the emission was passed through another appropriate filter (CO470) placed before the detector in order to eliminate scattered excitation light and visible light. The signal was detected by a Hammamatsu 956 photomultiplier tube connected to a Tektronix model 1912 transient digitizer. The decay trace was then digitalized and transferred to a computer for data processing.

Materials. The dyes 2,3,7,8,12,13,17,18-octaethyl-21H,23H-porphine platinum(II) (platinum(II) octaethylporphine; PtOEP), platinum(II) meso-tetraphenylporphine (PtTPP), and platinum meso-tetrakis(pentafluorophenyl)porphine (PtTFPP) were purchased from Porphyrin Products, Frontier Scientific Inc. (Logan, UT). 2,3,7,8,12,13,17,18-Octaethyl-21H,23H-porphine palladium(II) (palladium(II) octaethylporphine, PdOEP), tris(1,10-phenanthroline)-ruthenium(II) dichloride hydrate ($[Ru(phen)_3]Cl_2$), and tris(2,2′-bipyridyl)ruthenium(II) dichloride hexahydrate ($[Ru(bpy)_3]Cl_2$) were purchased from Aldrich. All the above dyes were used without further purification. Tris(4,7-diphenyl-1,10-phenanthroline)ruthenium(II) dichloride ($[Ru(dpp)_3]Cl_2$) and $[Ru(phen)_2phenCH_3]Cl_2$ (phen = 1,10-phenanthroline, $phenCH_3$ = 4-methyl-1,10-phenanthroline) were synthesized in Prof. Manners' group as previously described.[40]

Poly(sodium 4-styrenesulfonate) (PSS, M_w 70000), poly(allylamine hydrochloride) (PAH, Mw 70000), and polyethyleneimine (PEI, M_w 750000, 50 wt % solution) were purchased from Aldrich. 1,1,1-Trichloroethane (TCE, 99+%) and methanol (99%) were obtained from Aldrich. Deionized water (>10 MΩ cm) was obtained through the treatment of distilled water by a MilliQ Water System. Oxygen (Research Grade 4.7, 99.997%) and compressed dry air (impurity H_2O 10 ppm) were obtained from BOC gas.

Preparation of Mesoporous Silica Particles. The SBA-15 mesoporous silica particles were prepared according to a reported procedure[41,42] as follows: Pluronic P123 triblock copolymer (4.0 g, poly(ethylene oxide-*b*-propylene oxide-*b*-ethylene oxide), EO_{20}-$PO_{70}EO_{20}$, M_w = 5800, Aldrich) was added to a mixture of water (30 g) and aqueous HCl (2 M, 120 g) in a polypropylene autoclave and was stirred at 35 °C. In general, a clear solution was obtained in 1 h. Then, tetraethyl orthosilicate (TEOS, Aldrich, 99+%, 8.5 g) was added to the block copolymer solution under vigorous stirring. The mixture was continuously stirred for 5 min. Then the homogeneous solution was kept at 35 °C for 20 h without stirring, followed by aging at 90 °C for 2 days under quiescent conditions. The solid product was collected by filtration, washing with water, and then drying at 140 °C for 4 h. To remove the surfactant, the as-synthesized white powder solid was subjected to calcination at 550 °C with air flow for 6 h, in which the temperature ramp is 4 h. Nitrogen sorption experiments (T = 77 K) and scanning electron microscopy (SEM) imaging were employed to characterize the calcined silica material.

Preparation of Mesoporous Silica Particles on Layer-by-Layer Self-assembled Films (LbLSAF). Corning micro slides (No. 2947, plain, 3 in. × 1 in., thickness: 0.96−1.06 mm) were cut into 0.75 in. × 1 in. pieces and treated with a mixture of NH_4OH (29 wt %, Aldrich), H_2O_2 (30 wt %, Aldrich), and H_2O (1:1:5) at 70 °C for about 30 min, followed by a thorough rinse with deionized water and then ultrasonication in deionized water for 15 min. The films were stored in deionized water. The following solutions were used for layer-by-layer deposition: PSS solution (10 mM), PAH solution (10 mM), and PEI solution (10 mM).

Layer-by-layer films were prepared by spin coating. To form the first layer, the PEI solution (ca. 5 drops, 10 mM) was dropped

(32) Carraway, E. R.; Demas, J. N.; DeGraff, B. A. *Langmuir* **1991**, *7* (12), 2991−2998.
(33) (a) Demas, J. N.; DeGraff, B. A.; Coleman, P. A. *Anal. Chem.* **1999**, *71*, 793A-800A. (b) Demas, J. N.; DeGraff, B. A.; Xu, W. *Anal. Chem.* **1995**, *67* (8), 1377−1380. (c) Carraway, E. R.; Demas, J. N.; DeGraff, B. A.; Bacon, J. R. *Anal. Chem.* **1991**, *63* (4), 337−342. (d) Carraway, E. R.; Demas, J. N.; DeGraff, B. A. *Anal. Chem.* **1991**, *63* (4), 332−336.
(34) Wheeler, J.; Thomas, J. K. *J. Phys. Chem.* **1982**, *86* (23), 4540−4544.
(35) Thomas, J. K. *Acc. Chem. Res.* **1988**, *21* (7), 275−280.
(36) Zhang, H.; Sun, Y.; Ye, J.; Bian, H.; Zhang, P.; Wang, Y. *Xiangshan Science Conference on Functional Supramolecular System*, China, 2004.
(37) Barrett, E. P.; Joyner, L. G.; Halenda, P. P. *J. Am. Chem. Soc.* **1951**, *73* (1), 373−380.
(38) Brunauer, S.; Emmett, P. H.; Teller, E. *J. Am. Chem. Soc.* **1938**, *60* (2), 309−319.
(39) (a) Gregg, S. J.; Sing, K. S. W. *Adsorption, Surface Area and Porosity*, 2nd ed.; Academic Press: London, 1982. (b) Sing, K. S. W.; Everett, D. H.; Haul, R. A. W.; Moscou, L.; Pierotti, R. A.; Rouquérol, J.; Siemieniewska, T. *Pure Appl. Chem.* **1985**, *57* (4), 603−619.
(40) Lin, C.-T.; Böttcher, W.; Chou, M.; Creutz, C.; Sutin, N. *J. Am. Chem. Soc.* **1976**, *98* (21), 6536−6544.
(41) Kruk, M.; Jaroniec, M.; Ko, C. H.; Ryoo, R. *Chem. Mater.* **2000**, *12* (7), 1961−1968.
(42) Sayari, A.; Han, B.-H.; Yang, Y. *J. Am. Chem. Soc.* **2004**, *126* (44), 14348−14349.

onto a cleaned glass slide, which was placed on the flat surface of the vacuum chuck of the spinner. This solution wetted the glass surface completely. Spinning was initiated and maintained at 4000 rpm for 15 s. Then, some deionized water (ca. 5 drops) was placed on the slide, and it was spun (4000 rpm, 15 s) and allowed to dry. The washing procedure was repeated once again. To form the second layer, the PSS solution (ca. 5 drops, 10 mM) was placed on the substrate and spun, followed by two washing steps with deionized water as described above. Each subsequent layer was applied in the same series of three steps. This procedure was used to form the third layer, using the PAH solution (ca. 5 drops, 10 mM). Then two additional pairs of layers were deposited by alternately coating with the solutions containing PSS and PAH with intermittent washing steps. The top layer of the LbLSAF was designed to be PAH to impart a cationic charge to the surface. The surface will be attractive to the mesoporous silica particles, due to the negative charge of a silica nanoparticle surface. In general, we prepared the LbLSAF with three PSS/PAH bilayers, i.e., PEI−$(PSS-PAH)_3$. To form the final layer, an aliquot of the silica particle suspension (ca. 5 drops, ca. 10 mg/mL) was dropped onto the LbLSAF, and the slide was spun for 15 s at 4000 rpm, followed by two washing steps with deionized water as described above. After drying in air, the films obtained were further dried in a vacuum oven (<1 Torr) at 60 °C for 2 days.

Dyes were incorporated into the films by dipping them for about 5 min into clear solutions of the dyes at a concentration of ca. 1×10^{-4} M in various solvents. For the platinum dyes, the dyes were dissolved in 1,1,1-trichloroethane (TCE). $[Ru(dpp)_3]Cl_2$ was dissolved in methanol to form a clear solution ($\sim 10^{-4}$ M). The other three ruthenium dyes were dissolved in deionized water. The films were then allowed to dry in the dark overnight.

Luminescence Intensity and Decay Measurements. For steady-state PL measurements, an LbLSAF film was placed in a closed vacuum/pressure chamber and fitted into the optical path of the fluorescence spectrometer. The slits for the excitation monochromator were set at 4 nm and those of the emission monochromator were 8 nm. Samples were measured in the reflectance mode with right angle detection, and the signal intensity was recorded in the S&R (signal and reference) mode in 1.0 nm steps. To ensure the linearity of response, the sample source signal was always maintained to be less than 2×10^5 count s^{-1}. After each change in pressure, the sample was allowed to equilibrate for 10 min before the next luminescence measurement was carried out. Gas pressure was measured by an MKS Baratron 626A 13TAE absolute pressure transducer (1000 Torr with an accuracy of ±0.25% of the reading, ±0.15% of the reading over the range of 10−1000 Torr). For quantitative intensity measurements, data were acquired in the time-base scan mode (fixed excitation and emission wavelengths) at one point per second, for 300 s. Then the average emission intensity was calculated from these data. This data acquisition technique improves the precision of the intensity measurements, with a typical precision better than ±2% except at very high oxygen partial pressures when the residual PL intensity was very weak. A similar vacuum/pressure sample chamber was used for the pulsed laser experiments. It was equipped with an MKS Baratron 626A 12TAD absolute pressure transducer with similar specifications to that used for steady-state measurements.

Data Analysis. In fluid solution, luminescence intensities and decay times for quenching by oxygen follow the simple Stern−Volmer equation.[43]

$$\frac{I^o}{I} = \frac{\tau^o}{\tau} = 1 + k_q \tau^o [Q] \tag{1}$$

where I and τ are, respectively, the luminescence intensity and the luminescence decay lifetime, and the values superscripted with "o" refer to values in the absence of quencher. [Q] denotes the molar concentration of the quencher and k_q is the rate constant of the bimolecular quenching reaction. When the quencher is a gas such as oxygen, the luminescence intensity will, for simple systems (i.e., liquids, and solids far from saturation), be proportional to the partial pressure of oxygen, p_{O_2}, which, in turn, is proportional to the oxygen concentration. Here one can write

$$\frac{I^o}{I} = 1 + K_{SV} p_{O_2} \tag{2}$$

where the Stern−Volmer constant K_{SV} contains all of the proportionality constants relating the external oxygen pressure to the luminescence intensity. In our experiments, values of the unquenched intensity I^o and the unquenched lifetime τ^o were obtained at the lowest pressure accessible in our system, 0.2 and 0.06 Torr using the degassing system in the steady-state and time-resolved fluorometer, respectively.

Dyes in homogeneous solutions normally exhibit simple exponential luminescence decays. For the dyes adsorbed to the silica surface, almost all of the phosphorescence decays were nonexponential. The decay profiles were fitted to the general expression

$$I(t) = \sum_i A_i \exp\left(-\frac{t}{\tau_i}\right) \tag{3}$$

where $I(t)$ is the luminescence intensity from the dyes in the film at time t under a particular pressure and A_i is the pre-exponential factor for the ith species with a phosphorescence lifetime τ_i. For all of the decays reported here two exponential terms were sufficient to give a reasonable fit to the data. Intensity-weighted mean decay times $\langle\tau^o\rangle$ and $\langle\tau\rangle$ at various oxygen partial pressures were calculated with the expression

$$\langle\tau\rangle = \sum_i A_i \tau_i \tag{4}$$

in which the pre-exponential A_i factors were normalized, i.e., $\sum_i A_i = 1$. Lifetime Stern−Volmer plots were obtained from plots of $(\langle\tau^o\rangle/\langle\tau\rangle)$ against p_{O_2}.

Results and Discussion

Preparation of LbLSAF Containing Mesoporous Silica Particles. The SBA-15 mesoporous silica particles obtained are relatively monodisperse rods, and ca. 1 μm in length and 300 nm in diameter. Figure 1 shows the SEM images of the calcined SBA-15 mesoporous silica particles, in which Figure 1B was obtained for the selected area in Figure 1A at higher magnification. The particles possess two-dimensional hexagonal mesopores, which are parallel to the axis of the silica rod. Figure 2 shows a typical nitrogen sorption isotherm for the SBA-15 materials, which is similar to that reported previously.[30,41] The condensation processes occur in the relative pressure range of 0.74−0.80, and this very narrow range indicates that the mesoporous material possesses a very narrow pore size distribution. Furthermore, the hysteresis loop is narrow and symmetric, also indicating that the pore size distribution is narrow. The inset in Figure 2 shows the BJH pore size distribution calculated from the adsorption

(43) Lakowicz, J. R. *Principles of Fluorescence Spectroscopy*, 2nd ed.; Kluwer Academic/Plenum Publishers: New York, 1999.

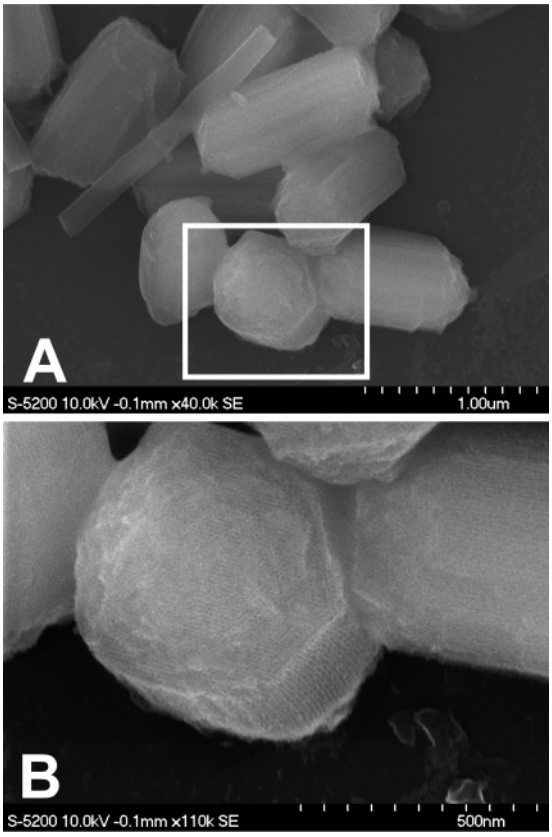

Figure 1. Scanning electron microscopy (SEM) image (A) of SBA-15 mesoporous silica particles; the bottom image (B) was obtained at higher magnification. The scale bar represents (A) 1.00 μm and (B) 500 nm.

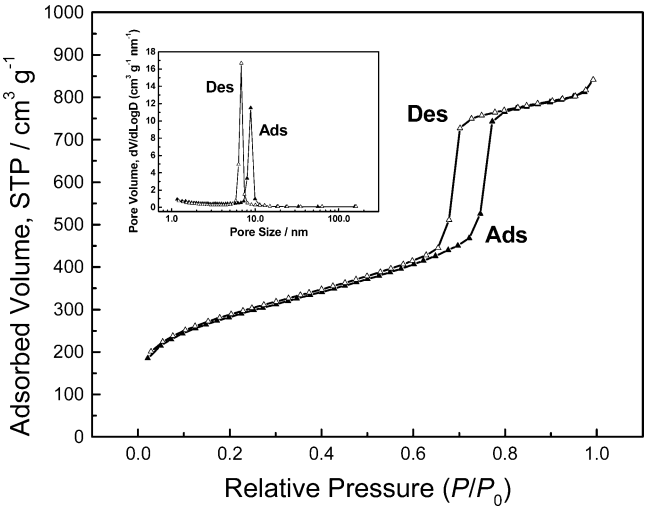

Figure 2. Nitrogen adsorption−desorption isotherms for SBA-15 mesoporous silica nanorods; inset: BJH pore size distribution obtained from the adsorption and desorption branches, respectively (adsorption, solid triangles; desorption, open triangles).

and desorption branches. It confirms the narrow pore size distribution, in which the peak width at half-height is only 0.8 nm. The BET surface area is 960 m^2/g, the pore size is 8.9 nm (from the adsorption branch), and the pore volume is 1.24 cm^3/g at the relative pressure of 0.95.

Layer-by-layer self-assembled films were prepared by the spin-coating method.[44] The authors of ref 44 have argued that this approach offers various advantages over the more common dipping method. Since we are using the LbLSAF film as an adhesion layer to attach the mesoporous silica

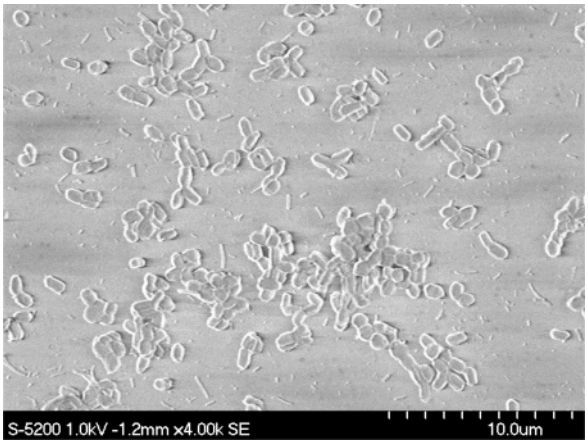

Figure 3. Scanning electron microscopy (SEM) images of mesoporous silica particles deposited on the layer-by-layer self-assembled film.

Chart 1. Schematic Structures of the Polyelectrolytes

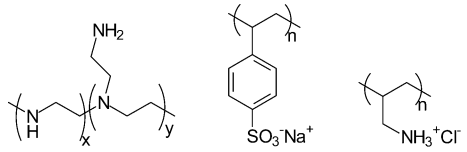

particles to a flat substrate, the key feature of these films for us is the ease and reproducibility of preparation. To create a negatively charged surface on the glass substrate, the glass slide was treated with an $NH_4OH-H_2O_2-H_2O$ mixture. The treated glass substrate was then coated with a layer of PEI, which acts as an adhesion promoter for the subsequently deposited PSS layer.[45] In the experiments described here, we prepared the LbLSAFs with one layer of PEI and three bilayers of PSS/PAH. Then, the negatively charged mesoporous silica particles were deposited on the positively charged PAH layer. The chemical structures of the polyelectrolytes are shown in Chart 1. The film formed was imaged by SEM. From the SEM images (Figure 3) of mesoporous silica particles deposited on the LbLSAF, one can see that the spin-coating approach leads to a submonolayer coverage of the LbL film by the rodlike silica particles.

The dyes were loaded into the mesoporous silica particles on the LbLSAF by dipping the dried films into the dye solution. Chart 2 shows the molecular structures of the dyes used in this study. Due to the high interior surface area of the mesoporous silica particles, and the small size of dye molecules as compared to the pore size (ca. 8.9 nm), we assume that all but a negligible fraction of the dye molecules are bound to the walls of the mesoporous channels. The amount of dye adsorbed to the silica particles is difficult to

(44) (a) Cho, J.; Char, K.; Hong, J.-D.; Lee, K.-B. *Adv. Mater.* **2001**, *13* (14), 1076−1078. (b) Chiarelli, P. A.; Johal, M. S.; Casson, J. L.; Roberts, J. B.; Robinson, J. M.; Wang, H.-L. *Adv. Mater.* **2001**, *13* (15), 1167−1171. (c) Lee, S.-S.; Hong, J.-D.; Kim, C. H.; Kim, K.; Koo, J. P.; Lee, K.-B. *Macromolecules* **2001**, *34* (16), 5358−5360. (d) Chiarelli, P. A.; Johal, M. S.; Holmes, D. J.; Casson, J. L.; Robinson, J. M.; Wang, H.-L. *Langmuir* **2002**, *18* (1), 168−173. (e) Sohn, B.-H.; Kim, T.-H.; Char, K. *Langmuir* **2002**, *18* (21), 7770−7772.

(45) (a) Krass, H.; Papastavrou, G.; Kurth, D. G. *Chem. Mater.* **2003**, *15* (1), 196−203. (b) Liu, S.; Kurth, D. G.; Möhwald, H.; Volkmerm, D. *Adv. Mater.* **2002**, *14* (3), 225−228.

Chart 2. Molecular Structures of the Phosphorescent Dyes

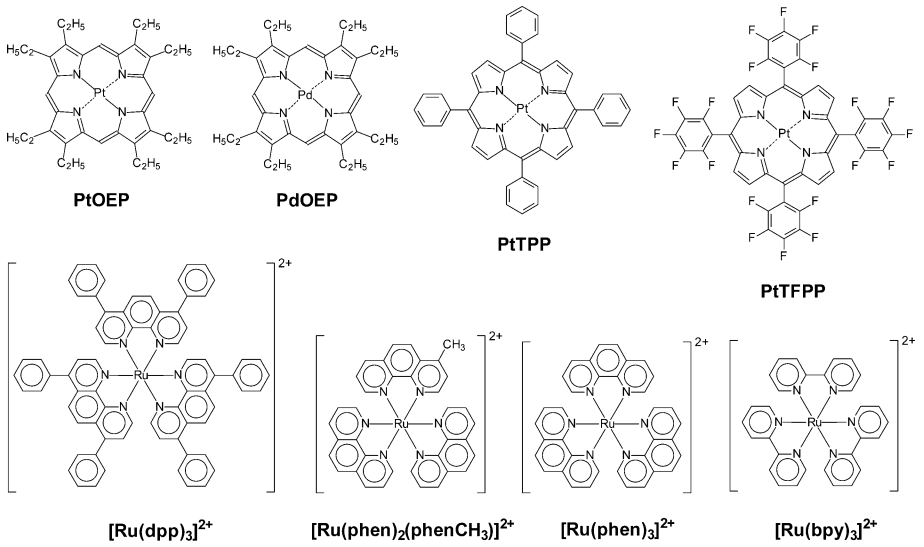

quantify. The luminescence intensity increased with time of exposure to the dye solution and with the concentration of the dye in the dipping solution, and the choice of conditions reported here was based on obtaining reasonable PL intensities and PL spectra for the dyes that resembled their spectra in solution. A number of control experiments were carried out to support the idea of dye absorption into the silica pores. For example, if the cationic ruthenium dye were adsorbed by dipping directly onto the anionic surface of a similar LbLSAF film, the luminescence intensity was too weak to be quantified. In another set of experiments, we replaced the mesoporous silica particles with nonporous spherical silica particles with a diameter of ca. 137 nm. Here too, for dyes adsorbed to this substrate, we observed only very weak PL intensity in the absence of oxygen.

Properties of the Dyes Adsorbed to the Films. The emission and excitation spectra of PtOEP deposited on the mesoporous silica film are shown in Figure 4A. The excitation spectrum shows two bands, 535 and 499 nm, due to the $^1S_0 \rightarrow {}^1S_1$ (π,π^*) transition, as well as the Soret band at 381 nm. The excitation spectra of PtTFPP and PtTPP on the mesoporous silica film resemble those of PtOEP, but the band positions of PtTFPP and PtTPP are bathochromically shifted by a few nanometers. The bathochromic shift of PtTPP is somewhat larger, and the peak at 540 nm has a much smaller intensity relative to that of the peak at 510 nm. The emission peak of PtOEP is at 646 nm. The corresponding emission peak of PtTFPP is at 649 nm, while that of PtTPP is at 661 nm. These spectra are very similar to the corresponding spectra of these dyes in simple solutions. We list the key peak positions in Table 1 and compare these values to those of the dyes in a polar aprotic polymer solution (poly(*n*-butylaminothionylphosphazene), C_4PATP),[25] in which these dyes are believed to be molecularly dissolved.

The emission and excitation spectra of the four ruthenium(II) complex dyes $[Ru(dpp)_3]Cl_2$, $[Ru(phen_2phenCH_3)]Cl_2$, $[Ru(phen)_3]Cl_2$, and $[Ru(bpy)_3]Cl_2$ in the mesoporous silica film are very similar. The emission and excitation spectra of $[Ru(phen)_3]Cl_2$ are shown in Figure 4B, and the corresponding peak positions are listed in Table 1.

With one exception, the phosphorescence decay profiles of all of the dyes investigated in the mesoporous silica films were nonexponential, both in the absence and the presence of oxygen. The exception is the decay profile of $[Ru(bpy)_3]Cl_2$ in the absence of oxygen, which fits very well to a single exponential form. All of the other decay profiles fit well to a sum of two-exponential terms, and for these samples, intensity-weighted mean lifetimes were calculated (eq 4). The unquenched mean decay times are also listed in Table 1. PdOEP has the longest lifetime, ca. 1 ms, whereas the

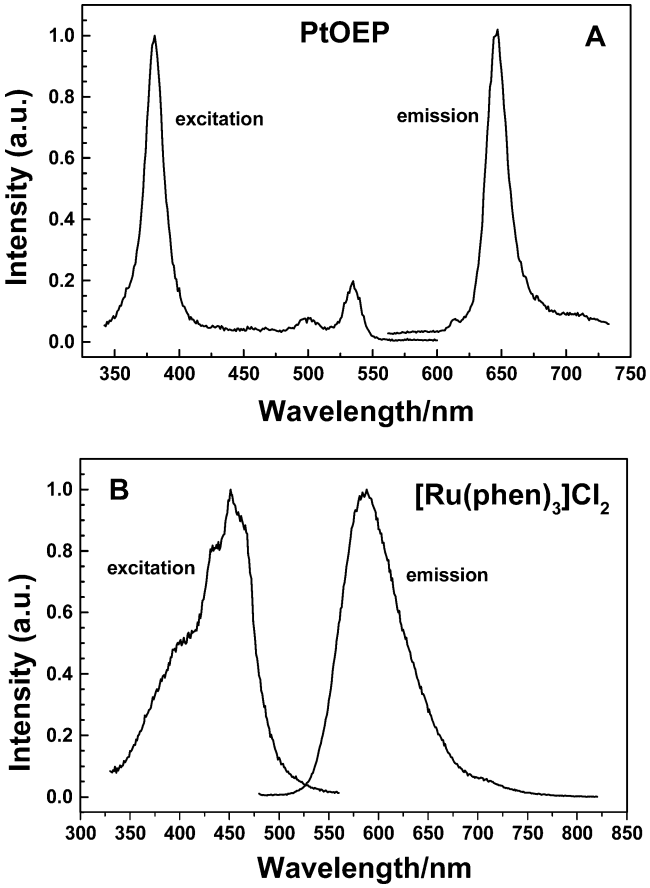

Figure 4. Emission and excitation spectra of dyes in the mesoporous silica particles on the LbLSAF: (A) PtOEP and (B) $[Ru(phen)_3]Cl_2$.

Table 1. Excitation, Emission Peak Positions, and the Unquenched Average Lifetimes of Various Dyes in the Mesoporous Silica Particles

	$\lambda_{ex.max}$ (nm)	$\lambda_{em.max}$ (nm)	$\langle\tau^o\rangle^a$ (μs)	$\tau_m^{o\ b}$ (μs)	γ^b	αR_{eff} (nm)
PdOEP	393	664	1000	687	0.94	0.38
PtOEP[c]	381	646	84.4	81.3	0.66	1.0
PtTFPP[c]	391	649	71.2	70.3	0.28	0.42
PtTPP	400	661	77.6	74.3	0.72	0.45
$[Ru(dpp)_3]Cl_2$[c]	465	603	7.56	7.11	0.48	0.90
$[Ru(phen_2phenCH_3)]Cl_2$	452	591	3.75	3.33	0.75	0.88
$[Ru(phen)_3]Cl_2$	451	586	2.99	2.67	0.73	1.25
$[Ru(bpy)_3]Cl_2$	452	600	1.40	1.40	0.14	1.12

[a] The unquenched mean lifetime calculated via eq 4. [b] The unquenched Gaussian lifetime ($p_{O_2} = 0$) calculated as described in ref 26, and the corresponding distribution parameter γ. [c] Peak maxima in C_4PATP: PtOEP, λ_{ex} 383 nm, λ_{em} 645 nm; PtTFPP, λ_{ex} 392 nm, λ_{em} 649 nm; $[Ru(dpp)_3]Cl_2$, λ_{ex} 460 nm, λ_{em} 605 nm. Data from ref 25.

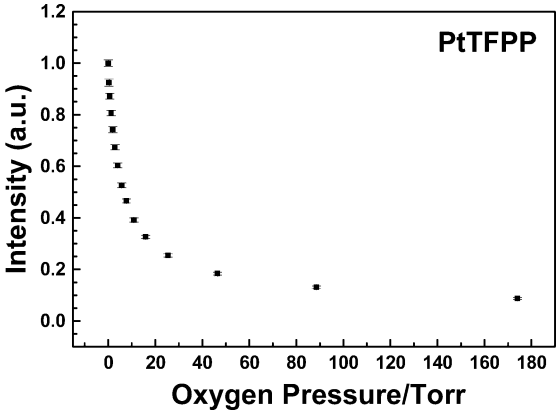

Figure 5. Variation in the PL intensities of PtTFPP in the mesoporous silica particles at various oxygen pressures.

platinum(II) dyes have lifetimes of tens of microseconds, and the lifetimes of the ruthenium(II) dyes are only several microseconds. $[Ru(bpy)_3]Cl_2$ has the shortest lifetime in the absence of O_2, only 1.40 μs.

Phosphorescence Quenching Experiments. In the presence of increasing partial pressure of oxygen, the PL intensity of the dyes decreases. An example is shown in Figure 5 for PtTFPP in the mesoporous silica film. Error bars are also included in the figure. It is evident that the relative error is very small (<2%). The degree of change varies from dye to dye, and not unexpectedly, the longer the unquenched lifetime of the dye, the greater the extent of quenching for a given value of p_{O_2}.

These data were then plotted against oxygen pressure according to eq 2. These Stern−Volmer (SV) plots for the platinum and palladium porphine dyes are presented in Figure 6A, and corresponding plots for the ruthenium dyes are presented in Figure 6B. All of the plots exhibit a downward curvature, especially in the lower range of oxygen pressures. This type of curvature has been seen previously for oxygen quenching of dyes adsorbed to a fumed silica, and the origin of the curvature has been attributed to a distribution of environments on the surface of the silica.[32] Despite the curvature, one expects (cf., eq 1) that the main difference in the sensitivity to quenching of the different dyes is the unquenched PL lifetime. For example, the Thomas group (Krasnansky et al.[26]) compared the sensitivity to oxygen quenching of two fluorescent dyes with very different

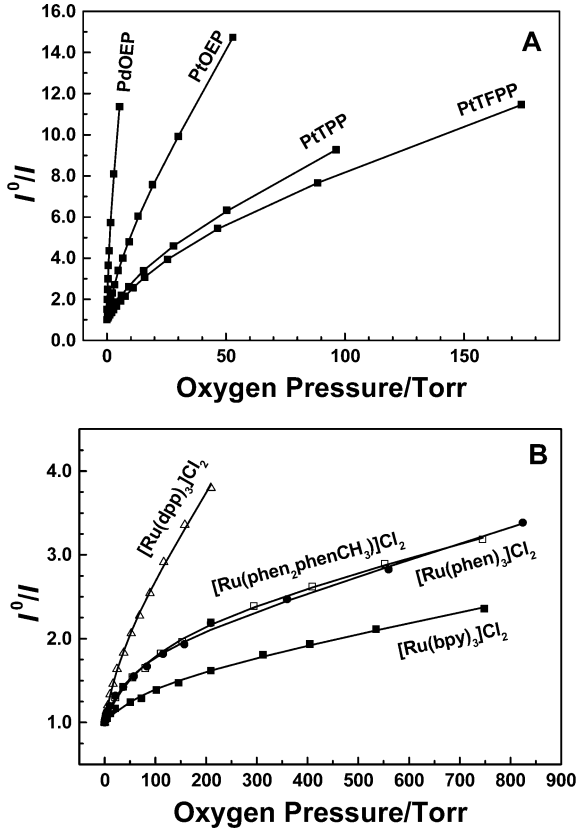

Figure 6. Intensity Stern−Volmer plots for four porphyrin dyes (A) and four ruthenium dyes (B: $[Ru(dpp)_3]Cl_2$, open triangles; $[Ru(phen)_2phenCH_3]Cl_2$, open squares; $[Ru(phen)_3]Cl_2$, solid circles; $[Ru(bpy)_3]Cl_2$, solid squares) in the mesoporous silica particles.

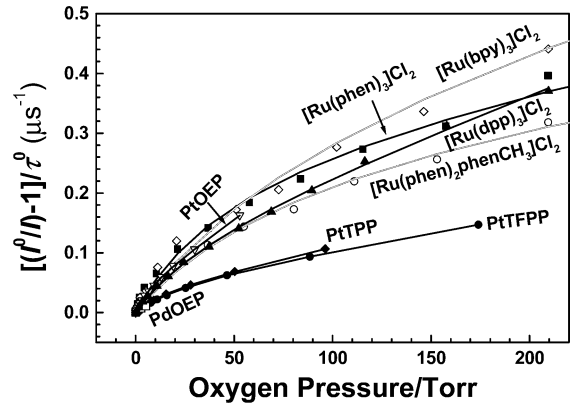

Figure 7. Intensity Stern−Volmer plots scaled by the reciprocal unquenched lifetime τ^o for different dyes in the mesoporous silica.

lifetimes, 9,10-diphenyl anthracene and pyrene, adsorbed to the surface of silica. Even though the individual PL decays were nonexponential, the I^o/I values, normalized by the difference in mean lifetime, fell on a common plot. We carry out a similar exercise in Figure 7, where we plot $[(I^o/I) - 1]/\langle\tau^o\rangle$ against oxygen partial pressure. We see that that this renormalization of the data brings the plots closer together, but that significant differences remain. This is a topic we will return to later in the paper.

In Figure 8, we show the PL decay curves for PtOEP for a series of experiments at increasing p_{O_2} values. All of the semilogarithmic decay plots are curved, but are easily fitted to a sum of two exponential terms. The decay rate of the excited state is substantially enhanced in the presence of

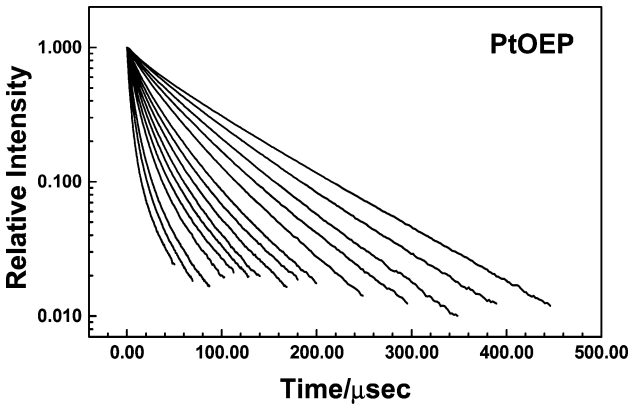

Figure 8. Semilogarithmic plots of phosphorescence decay profiles of PtOEP in mesoporous silica particles at various oxygen pressures.

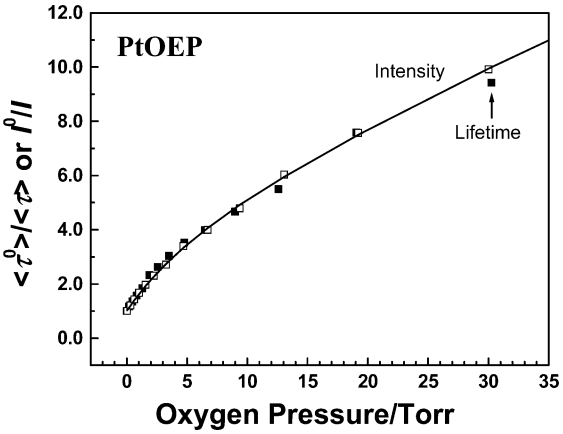

Figure 9. Comparison of intensity and lifetime Stern−Volmer plots of PtOEP in mesoporous silica particles.

increasing oxygen partial pressure. The PL decay curves for all of the dyes examined were similar in shape and showed increased decay rates in the presence of increasing oxygen pressure. The quenched PL decay rates for $[Ru(bpy)_3]Cl_2$, $[Ru(phen_2phenCH_3)]Cl_2$, and $[Ru(phen)_3]Cl_2$ became too rapid for accurate data collection with our instrumentation, and thus the only decay profiles measured for these dyes were those in the absence of oxygen.

In Figure 9, we compare plots for PtOEP of $\langle\tau^o\rangle/\langle\tau\rangle$ and I^o/I against p_{O_2}. These plots are coincident over the entire low-pressure range. At higher pressures (here for $p_{O_2} > 30$ Torr), the lifetime ratios fall below the intensity data. Similar results were obtained for the other platinum and palladium dyes and for $[Ru(dpp)_3]Cl_2$. We obtained nearly coincident plots $\langle\tau^o\rangle/\langle\tau\rangle$ and I^o/I against p_{O_2} for low to moderate extents of quenching, and at higher oxygen pressures, the lifetime ratio data exhibited a greater curvature, and the data points were below the intensity ratio points. For completeness, we present additional plots in the Supporting Information that accompanies this paper.

Interpreting the Phosphorescence Quenching Experiments. The experimental observation of nonexponential decays of dyes adsorbed to the silica surface points to a distribution of dye environments. This type of phenomenon has been seen previously in experiments from the Demas group and by the Thomas group. The two groups examined somewhat different silica samples. The former (Carraway et al.[31]) examined transparent disks prepared in a KBr press from a commercial porous fumed silica powder (Cab-O-Sil M-5, Cabot Corp., surface area 200 m^2/g before pressing, 190 m^2/g in the disk itself), whereas the latter (Krasnansky et al.[26]) examined a fumed silica (Cab-O-Sil HS-5) consisting of 8 μm diameter particles with a surface area of 325 m^2/g. It is likely that the surfaces of these silica samples are somewhat different. From the comment in Carraway et al.[32] that their ruthenium dye decay profiles "could all be accurately reproduced with a sum of three or four exponential terms," we infer that the dyes on the surface of the fumed silica had a much broader distribution of decays than we find for our mesoporous silica sample, where there were only slight deviations from an exponential fit, and two exponential terms were always sufficient to reproduce the decays. Because of a difference in data analysis strategy of the Thomas group, a direct comparison with their fluorescence decay profiles is more difficult, but the shape of these decay profiles in the absence of oxygen seem more consistent with the nearly exponential profiles that we find for our sol−gel mesoporous silica samples.

Phenomenological Models. The Demas group employed a phenomenological approach to data analysis. They interpreted the intensity SV data for oxygen quenching of ruthenium dyes on a silica surface in terms of the simple two-site model proposed by Demas and DeGraff[33] for microheterogeneous systems.

$$\frac{I^o}{I} = \frac{1}{\dfrac{f_1}{1 + K_{SV1}p_{O_2}} + \dfrac{1 - f_1}{1 + K_{SV2}p_{O_2}}} \tag{5}$$

This model is formulated in terms of two classes of binding sites, each with its own SV constant K_{SV1} and K_{SV2} and fractions f_1 and f_2 ($f_2 = 1 - f_1$) of the dye present at each site. The data in Figure 6 fit very well to this model, and the fitting parameters obtained are listed in Table 2. The fundamental assumption associated with this model is that f_1 and f_2 are properties of the dyes and sites to which they are bound, whereas the SV constants are a measure of their sensitivity to quenching. In this respect, it is interesting to note that the f_1 values, representing the sites more sensitive to quenching, are similar in magnitude for the four porphyrin dyes and range from 0.83 to 0.89. The situation is not quite so simple for the ruthenium dyes, and here f_1 values range from 0.39 for $[Ru(bpy)_3]Cl_2$ to 0.61 for $[Ru(dpp)_3]Cl_2$.

This approach to data analysis assumes that surface diffusion of oxygen bound to the surface of the silica is responsible for the quenching process. The surface concentration of quencher $[Q]_{ads}$ depends on the external oxygen pressure through the adsorption isotherm. Carraway et al.[32] measured the oxygen binding isotherm to their silica disks, but for the low fractional surface coverage θ accessible in their experiments, they could not distinguish a simple Langmuir isotherm (eq 6) from the more general Freundlich isotherm (eq 7). In the Langmuir isotherm, θ is related to p_{O_2} through the expression

$$\theta = \frac{[Q]_{ads}}{[Q]_{max}} = \frac{bp_{O_2}}{1 + bp_{O_2}} \tag{6}$$

Table 2. Comparison of Stern−Volmer Constants for Various Dyes in the Mesoporous Silica Particles on the LbLSAF Obtained from the Nonlinear Fitting Employing Different Models, i.e., Demas-DeGraff Two-Site Model and Freundlich Isotherm Model

	Demas-DeGraff two-site model				Freundlich isotherm model		
	f_1	K_{SV1}/Torr^{-1}	K_{SV2}/Torr^{-1}	χ^2	K'_{SV}	$1/n$	χ^2
PdOEP	0.89	6.37	0.16	0.0119	3.41	0.67	0.0397
PtOEP	0.87	0.63	0.017	0.00344	0.70	0.67	0.0117
PtTFPP	0.87	0.20	0.0060	0.00042	0.30	0.69	0.0123
PtTPP	0.83	0.29	0.012	0.00071	0.34	0.70	0.00459
$[Ru(dpp)_3]Cl_2$	0.61	0.054	0.0040	0.0008	0.064	0.71	0.0006
$[Ru(phen_2phenCH_3)]Cl_2$	0.58	0.025	0.00065	0.00073	0.063	0.54	0.00138
$[Ru(phen)_3]Cl_2$	0.50	0.036	0.00095	0.00134	0.059	0.55	0.00115
$[Ru(bpy)_3]Cl_2$	0.39	0.016	0.00076	0.00062	0.021	0.63	0.00019

where $[Q]_{max}$ is the maximum surface concentration (presumably a monolayer) and b is related to the adsorbate adsorption energy. The Langmuir model assumes that all binding sites have the same binding energy. The Freundlich model takes into account a distribution of sites with different binding energies, leading to an expression of the form

$$\theta = a\, p_{O_2}^{1/n} \tag{7}$$

for gas−solid adsorption. Here a represents a series of constants and n is an empirical parameter.

These authors describe their attempts to fit their intensity SV plots to a number of different models. In addition to the two-site model (eq 5) cited above, the other model that fit their data involved diffusional quenching by adsorbed oxygen in which oxygen adsorption followed the Freundlich isotherm. In the corresponding SV relationship,

$$\frac{I^o}{I} = 1 + K_{SV}[O_2]_{max} a p_{O_2}^{1/n} = 1 + K'_{SV} p_{O_2}^{1/n} \tag{8}$$

K'_{SV} is a fitting parameter that represents the product of K_{SV} and the constants $a[O_2]_{max}$. For the results reported by the Demas group, a similar expression based on the Langmuir isotherm of oxygen adsorption and a single Stern−Volmer constant could not accommodate the curvature seen in the I^o/I plots (cf., Figure 8 in ref 32) at low oxygen pressures. We see similar curvature in our data in Figure 7. Not surprisingly, our data also can be fitted very well to eq 8, and the fitting parameters we obtained for each dye are presented in Table 2. As the chi-squared values in Table 2 indicate, we obtain a very similar quality of fit of our data to eq 8 and to the two-site model, eq 5. The excellence of fit by itself, however, should not be taken as a proof that either model properly identifies the underlying mechanism of the quenching process in our experiments.

Carraway et al.[32] also commented that they could not fit their data to a Langmuir surface diffusion model in which they assume a Gaussian distribution of lifetime sites, with each site quenched with the same bimolecular rate constant. This Gaussian model was originally proposed by Albery et al.,[46] and, as we see in the following paragraphs, it was applied very effectively by the Thomas group to oxygen fluorescence quenching experiments for dyes adsorbed to Cab-O-Sil HS-5 silica particles.

(46) Albery, W. J.; Bartlett, P. N.; Wilde, C. P.; Darwent, J. R. *J. Am. Chem. Soc.* **1985**, *107* (7), 1854−1858.

The Gaussian Distribution Model. Krasnansky et al. invoked the idea of a Gaussian distribution of unquenched decay rates to interpret the nonexponential PL decay traces of 9,10-diphenylanthracene and pyrene adsorbed to silica.[26] This model has two fitting parameters, a Gaussian mean decay rate ($1/\tau_m$) and the width of the distribution (γ). In fitting their experiments, they found that both γ and the mean decay rate increased with increasing oxygen pressure. They carried out experiments over a wide range of temperatures (−92 to 18 °C) and showed that the SV slopes had much steeper slopes at lower temperature. They plotted their data against the bulk molar oxygen concentration, related to p_{O_2} via the ideal gas law, and attributed the enhanced quenching at lower temperature to enhanced oxygen adsorption to the silica surface. On this basis, they ruled out a quenching mechanism involving direct collision of gaseous O_2 molecules with excited dyes on the silica surface.

To pursue their analysis further, they measured oxygen adsorption isotherms at four temperatures ranging from −98 to −47 °C. Over this temperature range, for their sample, the adsorption followed a simple Langmuir isotherm. They extrapolated these data to higher temperatures in order to estimate the amount of oxygen bound and the mean residence time of an oxygen molecule on the silica surface. With these data, they were able to show that their experiments at all temperatures were consistent with a quenching rate expression of the form

$$\frac{1}{\tau_m} = \frac{1}{\tau_m^o} + k'_q[O_2]_{ads} \tag{9}$$

where $1/\tau_m^o$ is the Gaussian mean decay rate for the dye in the absence of oxygen and k'_q is the second-order quenching rate constant. Plots of k'_q against oxygen surface concentration, calculated from the Langmuir binding isotherm, were linear and increased with temperature. This result shows that the steeper SV slopes at low temperature were due to an enhanced oxygen surface concentration and not a fundamental change in quenching mechanism. The calculated Arrhenius activation energy for k'_q was close in magnitude to the binding energy of oxygen on the surface of the silica.

One of the most interesting aspects of their paper concerns the nature of oxygen diffusion responsible for quenching. They commented that, from a steady-state point of view, the amount of oxygen adsorbed on the silica surface in the range where quenching occurs is quite low; at ambient temperatures, the surface quencher concentration even approaches the surface probe concentration. They also concluded that

the mean residence time that a given oxygen molecule resides on the surface is quite short, anywhere from a few picoseconds to several hundred picoseconds depending on the temperature. These short residence times would not be expected to yield the observed dynamic type of quenching if the oxygen molecules initially present on the surface at the moment of probe excitation were completely responsible for the quenching of the probe's excited state.[26] In their view, the dye molecules on the surface are relatively immobile. Oxygen molecules from the atmosphere rapidly diffuse onto and depart from the surface so that the number of times an adsorbed oxygen is replaced at some other arbitrary surface location by an oxygen from the gas phase is great during the lifetime of the probe. The random displacement is crucial in describing the apparent surface migration distance incurred during the lifetime of the dye's excited state.

We also fitted our decay curves to the Gaussian lifetime distribution model. Not having measured oxygen isotherm data, we do not attempt as deep an analysis of our data as that reported by Krasnansky et al.[26] We prefer to make more general comments about differences in the two approaches to treating data. In Table 1, we present values of τ_m^o and γ for each of the dyes we examined. With the exception of PdOEP, the Gaussian-weighted average lifetimes and the intensity weighted average lifetimes (eq 4) are similar in magnitude, but the Gaussian lifetime is always smaller. These mean lifetimes represent different averages over the decay rate distribution. We also note that the γ values for $p_{O_2} = 0$ are different for the different dyes, and there is no particular pattern that can be associated with molecular structure. This situation is different from that reported by Krasnansky et al.,[26] who reported very similar values ($\gamma = 0.49$) for both pyrene and diphenylanthracene fluorescence at 18 and 19 °C, respectively. In their experiments, γ values increased gradually with increasing oxygen partial pressure, whereas our results in fitting data to this model were not so simple. For the interested reader, we provide plots for PtOEP, PtTFPP, PtTPP, PdOEP, and $[Ru(dpp)_3]Cl_2$ of $1/\tau_m$ and γ vs p_{O_2} in Figure S1 of the Supporting Information accompanying this article. For the Pt dyes, values of the fitting parameter γ increase rapidly over a very small range (0−5 Torr) of low oxygen pressures. This indicates that the spread of the lifetime distribution increases, and possibly that not all sites are being quenched with the same efficiency. In contrast, γ values for the ruthenium dyes show substantial scatter, and no clear pattern emerges from the data as a function of increasing oxygen pressure.

In addition, plots of τ_m^o/τ_m (i.e., Gaussian mean lifetimes) are steeper than corresponding plots of $\langle\tau^o\rangle/\langle\tau\rangle$, whereas the latter, as we have seen in Figure 9, correspond rather well to plots of I^o/I. In the Supporting Information, we provide individual plots of I^o/I, $\langle\tau^o\rangle/\langle\tau\rangle$, and τ_m^o/τ_m, for each of the dyes for which we obtained PL decay profiles as a function of oxygen pressure (see Figure S2). Overall, we conclude that the PL decay profile fitting parameters from the Gaussian distribution model exhibit substantially more scatter and a less self-consistent variation with increasing oxygen pressure than the more phenomenological models described above.

Variation in Capture Radius for the Different Dyes. In this section, we return to the data in Figure 7 and address the question of why scaling the data by the lifetime of the dye is not sufficient to reduce the quenching data to a common line. To proceed, we introduce for comparison purposes the results of oxygen quenching experiments for these same dyes dissolved in a polymer film consisting of C_4PATP. One feature that these experiments have in common with oxygen quenching experiments for dyes adsorbed to the silica surface is that, on the time scale of the excited state lifetime, the dyes remain relatively immobile and quenching is dependent on oxygen diffusion. The polymer film acts as a viscous liquid, and for diffusion-controlled quenching in three dimensions, the diffusion-controlled rate constant k_q can be written as

$$k_q = 4\pi N_A \alpha R_{eff} D_{O_2} \tag{10}$$

Here N_A is Avogadro's number, D_{O_2} is the oxygen diffusion coefficient in the polymer, R_{eff} is the effective interaction distance between the excited dye and quencher at which quenching takes place, and α describes the fraction of encounters that lead to quenching.

Under these circumstances, one can write the Stern−Volmer equation as

$$\frac{1}{\tau^o}\left(\frac{I^o}{I} - 1\right) = 4\pi\alpha R_{eff} N_A P_{O_2} p_{O_2} \tag{11}$$

Here P_{O_2} is the oxygen permeability, equal to the product of D_{O_2} and the Henry's Law constant S_{O_2} relating the molar oxygen concentration in the film to the external oxygen pressure ($[O_2] = S_{O_2}\, p_{O_2}$). In reality, because of multiple collisions, the magnitude of αR_{eff} varies with factors such as temperature that affect diffusion rates in the system. In the limit of $D_{O_2} \rightarrow 0$, $\alpha \rightarrow 1$, and R_{eff} approaches the true capture radius. In more practical terms, a value for αR_{eff} can be determined (as for PtOEP in poly(dimethylsiloxane), PDMS) where the permeability of the polymer to oxygen is known independently. In treating oxygen quenching data for PtOEP in PDMS and C_4PATP at 23 °C, we have used the value $\alpha R_{eff} = 1.0$ nm.[25]

Examination of eq 11 indicates that, for a series of different dyes, $1/\tau^o$ itself may not be a sufficient scaling parameter to reduce all the data to a common line if the dyes differ in their αR_{eff} values. Indeed, for $[Ru(dpp)_3]Cl_2$ and a series of platinum porphine dyes in C_4PATP, we found that differences in slope of the linear Stern−Volmer plots could not be accounted for exclusively on the basis of differences in the unquenched lifetime. The data could be accommodated only in terms of differences in the quenching efficiency of the excited state of these dyes with oxygen as expressed by αR_{eff}. In this way we determined a value of $\alpha R_{eff} = 0.5$ nm for $[Ru(dpp)_3]Cl_2$ and 0.65 nm for PtTFPP in this matrix.[25]

This idea can be extended to the case of oxygen quenching for dyes adsorbed to the surface of mesoporous silica by seeking values of αR_{eff} that operate as scaling factors along the *y*-axis to bring the various quenching curves into proximity. In this instance, the parameter P_{O_2} in eq 11 no longer refers to the traditional "permeability" of a material

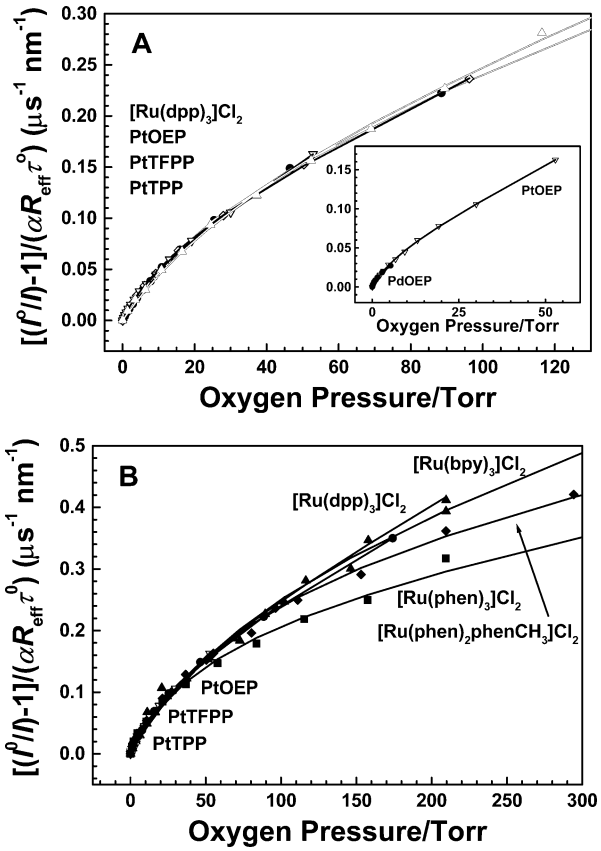

Figure 10. Scaled intensity Stern−Volmer plots (eq 11). The scaling parameter employed is the reciprocal of the product $\tau^o\alpha R_{eff}$. Values of αR_{eff} for each dye were selected relative to an assumed value of 1.0 nm for PtOEP to optimize superposition of the curves. Individual values of αR_{eff} for each dye are presented in Table 1. (A) Scaled plots for $[Ru(dpp)_3]Cl_2$ (filled triangles), PtOEP (open inverted triangles), PtTFPP (filled circles), PtTPP (open diamonds). The inset compares data for PdOEP (open circles) with that for PtOEP. (B). A corresponding plot at higher pressures that includes data for the four ruthenium dyes.

to oxygen, but rather represents all of the proportionality constants except αR_{eff} connecting the measurable parameters on the left-hand side of the equation to the external oxygen pressure.

In Figure 10 we show that, at low oxygen pressure, the quenching data for all of the dyes will fit a common curve if one plots $[(I^o/I) - 1]/(\alpha R_{eff}\tau^o)$ vs p_{O_2}, where the αR_{eff} values are taken relative to an assumed value of 1.0 nm for PtOEP as the best scaling factors for curve superposition. $[Ru(phen)_3]Cl_2$ shows a pronounced downward deviation from the master curve for p_{O_2} values above 40 Torr, and the structurally related $[Ru(phen_3phenCH_3)]Cl_2$ shows a similar effect for $p_{O_2} > 100$ Torr. The best fit αR_{eff} values are presented in Table 1. One sees that αR_{eff} values range from 0.38 for PdOEP, 0.42 for PtTFPP, and 0.45 for PtTPP to 0.95 for $[Ru(dpp)_3]Cl_2$ and 1.12 for $[Ru(phen_3phenCH_3)]Cl_2$. Lower values of αR_{eff} for PtTFPP and PtTPP are consistent with steric effects associated with the four phenyl substituents on the porphyrin ring decreasing the quenching efficiency per encounter, but this effect will not explain the low quenching per encounter for PdOEP. The main surprise in the data is that the value of αR_{eff} for $[Ru(dpp)_3]Cl_2$ is so similar to that of PtOEP. In C_4PATP films, this value is half that of PtOEP and signifies that, for diffusional quenching in three dimensions, the interaction between oxygen and the excited ruthenium dye is less efficient in deactivating the excited state than for PtOEP. The corresponding values for quenching on the silica surface indicate that, on a locally flat surface, these differences largely disappear.

Summary

We prepared a sample of mesoporous silica containing a narrow distribution of pore sizes with a mean pore diameter of 9 nm and a surface area of 960 m^2/g. The silica was prepared in the form of short rods of similar size, ca. 1 μm in length and 300 nm in diameter. Sensor films were prepared by adsorbing these particles at submonolayer coverage on a thin polymer film with a positively charged surface prepared by the layer-by-layer method. When these films were dipped into solutions of various dyes and the solvent was allowed to evaporate, the dyes became incorporated into the pores of the mesoporous silica particles. While dyes adsorbed to the layer-by-layer film itself had very weak photoluminescence intensity, dyes incorporated into the mesoporous silica-coated polymer films had an intense fluorescence that was easily detected.

The phosphorescent dyes employed were platinum and palladium porphines (PtOEP, PdOEP, PtTPP, and PtTFPP) and ruthenium complexes ($[Ru(dpp)_3]Cl_2$, $[Ru(phen)_2phenCH_3]Cl_2$, $[Ru(phen)_3]Cl_2$, and $[Ru(bpy)_3]Cl_2$). The phosphorescence-quenching behavior was investigated by monitoring the changes in phosphorescence emission intensity and lifetime upon varying the oxygen pressure. The PL emission intensities and decay lifetimes decrease with an increase in oxygen partial pressure. The quenching sensitivity increases with the unquenched lifetime of the dye. Overall, the data for these phosphorescent dyes resembled those described by the Demas group for ruthenium dyes adsorbed to transparent disks prepared by compression molding of porous fumed silica particles. The data did not fit as well to the Gaussian model used so effectively by the Thomas group to describe fluorescence quenching by oxygen on the surface of somewhat different silica particles. Our interests are more related to the functioning of these thin films as sensors rather than the detailed quenching mechanism by oxygen on the silica surface. In future publications, we will report the results of experiments that describe the rate of response of these sensors to a rapid change in oxygen pressure.

One interesting mechanistic aspect about the quenching process to emerge from our data is that the intensity and lifetime data we obtained for the different dyes (I^o/I, τ^o/τ) cannot be scaled to a common curve using the unquenched dye lifetime τ^o as the sole scaling parameter. A common curve can be obtained if we assume that the different dyes have different quenching probabilities per encounter with oxygen as expressed by values of αR_{eff}. Based on an assumed value of $\alpha R_{eff} = 1.0$ nm, corresponding values inferred for the other dyes were 0.9 nm for $[Ru(dpp)_3]Cl_2$, 0.42 for PtTPP, and 0.45 for PtTFPP.

Acknowledgment. The authors thank NSERC Canada and the Royal Canadian Mounted Police for their support of this

research. I.M. thanks NSERC Canada for a Canada Research Chair.

Supporting Information Available: The plots of $k_m = 1/\tau_m$ and γ values from the Gaussian distribution model against the oxygen pressure, and the comparison of intensity and (Gaussian) lifetime Stern−Volmer plots (PDF). This material is available free of charge via the Internet at http://pubs.acs.org.

CM047770K